Long-living periodic solutions of complex cubic-quintic Ginzburg-Landau equation in the presence of intrapulse Raman scattering: A bifurcation and numerical study

Ivan M. Uzunov,[1,2,*] Svetoslav G. Nikolov,[2,3] Todor N. Arabadzhiev,[1] and Zhivko D. Georgiev[4]
[1]*Department of Applied Physics, Faculty of Applied Mathematics and Informatics, Technical University of Sofia, 8 Kliment Ohridski Boulevard, Sofia 1000, Bulgaria*
[2]*Institute of Mechanics, Bulgarian Academy of Sciences, Academy Georgi Bonchev Strasse, Building 4, 1113 Sofia, Bulgaria*
[3]*Department of Mechanics, University of Transport, Geo Milev Strasse, 158, 1574 Sofia, Bulgaria*
[4]*Department of Theoretical Electrical Egineering, Technical University of Sofia, 8 Kliment Ohridski Boulevard, Sofia 1000, Bulgaria*

(Received 22 May 2024; accepted 30 July 2024; published 26 August 2024)

We have found long-living periodic solutions of the complex cubic-quintic Ginzburg-Landau equation (CCQGLE) perturbed with intrapulse Raman scattering. To achieve this we have applied a model system of ordinary differential equations (SODE). A set of the fixed points of the system has been described. A complete phase portrait as well as phase portraits near the fixed points have been built for a proper choice of parameters. The behavior of the model system near the fixed points has been determined. We have presented a detailed description of the subcritical Poincaré-Andronov-Hopf bifurcation due to the intrapulse Raman scattering that appears at one of the fixed points. We have established that there appears an unstable limit cycle in the SODE. To check the validity of the obtained results from the model system we have compared them with the results of the numerical solution of the CCQGLE perturbed with intrapulse Raman scattering. There has been found a remarkable correspondence between the obtained numerical results for the amplitude and frequency of the soliton pulses and the results for these parameters of the bifurcation theory. We have observed that the numerical characteristics of the propagating solitonlike pulses—amplitude, frequency, width, and position—periodically change if we change the distance with a period determined by the bifurcation analysis.

DOI: 10.1103/PhysRevE.110.024214

I. INTRODUCTION

In optics the complex cubic-quintic Ginzburg-Landau equation (CCQGLE) and the complex cubic Ginzburg-Landau equation (CCGLE) have been used to describe passive mode-locked both solid-state and fiber lasers [1–3] as well as the wave propagation in nonlinear optic fibers with gain and spectral filtering [4] (for a review see [5]).

The solutions of the CCGLE and CCQGLE can be divided into two classes: localized fixed-shape solutions and localized pulsating solutions. The CCQGLE has exact chirped solitary wave solutions [6–17] in both the negative and positive group velocity dispersion region [18–20]. The most typical solution in the case of CQ nonlinearity is a flat-top one derived in [7]. Different finite-dimensional models like the soliton perturbation theory [16,21], the method of moments [16,21–26], the variation method in [16,21], the method using average complex potentials [27], and others have been applied for the study of the solutions of the CCQGLE [16,21,28–30]. The numerical solutions of the CCQGLE have revealed the existence of localized pulsating solutions in the positive dispersion region [31]. They have also revealed the existence of localized pulsating solutions, such as plain pulsating, creeping, and erupting (exploding) solutions in the negative dispersion region [32,33]. The known exact solutions and the numerical solutions of the CCQGLE, as well as the stability of these solutions, have been reviewed in [16,17].

For the study of ultrashort optic pulses, it is necessary to include higher-order effects (HOE): third-order dispersion (TOD), self-steepening (SS), and intrapulse Raman scattering (IRS) [5,21,34–37]. The influence of the HOE on the localized fixed-shape solutions of the CCGLE has been studied in [38–41]. The influence of the HOE on the localized pulsating solutions of the CCGLE has been studied in [42,43].

A finite-dimensional dynamic system for the amplitude and frequency of the soliton solution of the CCGLE in the presence of HOE has been derived in [39,40,44,45]. The analysis of its stationary solutions as well as their stability has shown that narrowband filtering and nonlinear gain can control the self-frequency shift due to the IRS of ultrashort optical solitons [39,40]. Moreover, further analysis of the corresponding two-dimensional nonlinear ODE dynamic system has revealed the existence of Poincaré-Andronov-Hopf bifurcation concerning the parameter that describes the IRS [44,45]. Our aim here is to present an approach for the study of pulsating solutions of the CCQGLE in the presence of IRS. The core of our approach is the bifurcation analysis of the finite-dimensional dynamic system for the amplitude and frequency of the soliton solution.

Our study includes (1) making a detailed analysis of this local bifurcation of the appearance (birth) of limit cycle(s) from a singular (fixed) point of the focus or center type; (2) obtaining the structure of the boundaries of the stability and

*Contact author: ivan_uzunov@tu-sofia.bg

instability regions in the parameter space for equilibria and limit cycle(s) [periodic orbit(s)]; and (3) finding qualitative equivalence for the behavior of the CCQGLE and nonlinear ODE system when the effect of IRS is varied. Hence, the equilibria (fixed points) of the dynamic system have been found and the complete geometrical representation (phase portrait) has been described. Moreover, the phase portraits in the neighborhood of any fixed point have been built. Using the applied bifurcation theory [46–50], in terms of Lyapunov quantities [also called Lyapunov values (coefficients), or focus values], a detailed investigation of subcritical Poincaré-Andronov-Hopf bifurcation due to the intrapulse Raman scattering that appears around one of the fixed points has been performed. Our analysis has revealed the approximate parameters of the unstable limit cycle. However, we have also found a variety of long-living quasi-limit cycles close to the periodic solutions. The results from the bifurcation and phase analyses have been compared with the numerical results obtained from the solution of the CCQGLE. For the numerical solution of the CCQGLE we have used the iterative Agrawal method with one and two iterations [51,52]. There has been established a good quantitative correspondence between the results of the bifurcation theory and those of the numerical solution of the perturbed CCQGLE. We have succeeded in numerically finding a long-living unstable limit cycle in the CCQGLE predicted by the bifurcation theory. The reported results in this paper could be of interest and be used in different practical applications.

The paper is organized as follows: First, the physical meaning and applications of the generalized CCQGLE are presented in Sec. II. In Sec. III, a nonlinear system of ODEs is introduced which we use as a finite-dimensional model for the qualitative prediction of the CCQGLE behavior (solutions). In Sec. IV, the required magnitude parameters for the application of the bifurcation analysis are briefly described. Section V presents the results of the application of the bifurcation theory for the nonlinear ODE system. A detailed description of subcritical (hard loss of stability) Poincaré-Andronov-Hopf bifurcation due to the parameter describing IRS has been provided. Moreover, we have presented the numerical results of the basic equation (1). Thus, the general question about the applicability of finite-dimensional model predictions for the analysis of the CCQGLE solutions has been completely answered. Our conclusions are given in Sec. VI. Finally, the fixed points of the nonlinear ODE system have been calculated in the Appendix.

II. BASIC EQUATION

The dynamic behavior is described by the following complex cubic-quintic Ginzburg-Landau equation (CCQGLE) perturbed by IRS [1,2,3,4,5,16],

$$i\frac{\partial U}{\partial x} + \frac{1}{2}\frac{\partial^2 U}{\partial t^2} + |U|^2U = i\delta U + i\beta\frac{\partial^2 U}{\partial t^2} + i\varepsilon|U|^2U + i\mu|U|^4U + \gamma U\frac{\partial}{\partial t}(|U|^2), \quad (1)$$

where U is the normalized envelope of the electric field, t and x are the evolutional and spatial variables, δ is the linear loss-gain coefficient, β describes the spectral filtering (gain dispersion), ε is the nonlinear gain or absorption coefficient [13–15] (the nonlinear gain arises from the saturable absorption), and μ is the higher-order correction term to the nonlinear amplification or absorption [13–15] (if negative, it accounts for the saturation of the nonlinear gain [33]). In this equation we have implied that the group-velocity dispersion is anomalous. Parameter γ takes into account the effect of the IRS in the simplest quasi-instantaneous description. In this case there has been applied a linear approximation to the frequency-domain Raman response function [35–37,53]. For pulses shorter than 1 ps, the Raman gain (related to the frequency-domain Raman response function) does not vary linearly over the pulse bandwidth. Parameter γ could be treated as a fitting parameter [34]. Equation (1) presents a frame of reference moving with the pulse and it is a basically phenomenological model. There are a number of theoretical and practical issues to be considered to prove that Eq. (1) is a good qualitative model for the real mode-locked lasers. On the other hand, it has been proposed as a master equation for solid-state lasers with fast saturable absorber [1–3] as well as for the mode-locked fiber lasers [54]. It should be noted that the relations between the physical parameters describing a ring fiber laser mode locking through nonlinear polarization rotation and the coefficients of the CCQGLE have been given in [55].

To complete the numerical solution of Eq. (1), we have used the Agrawal split-step Fourier method with one and two iterations [51,52]. In some cases (see below), the fourth-order Runge-Kutta in the interaction picture (RK4IP) method has also been applied. The numerical parameters used in our calculation are as follows: time resolution: 0.002 44, number of samples: 2^{15}, and a constant propagation step (but case dependent)—with size between 10^{-3} and 5×10^{-4}. The initial condition used for the calculation of Eq. (1) is as follows: $U(0,t) = \eta_0 \mathrm{sech}[\eta_0 t]\exp[-i\omega_0 t]$, where $\eta(x_j) = \max|U(x_j,t)|, \forall t$ is the peak amplitude; $\eta_0 = \eta(0)$; $\omega(x_j) = \sum_{i=0}^{N-1}\omega_i|U(x_j,\omega_i)|^2/\sum_{i=0}^{N-1}|U(x_j,\omega_i)|^2$ is the mean circular frequency; $\omega_0 = \omega(0)$; $\tau(x_j) = (\sum_{i=0}^{N-1} t_i|U(x_j,t_i)|^2/\sum_{i=0}^{N-1}|U(x_j,t_i)|^2)$ is the time position; $r(x_j) = \tau(x_j) - \tau_R(x_j)$ is the residual of the linear fit of the position, in which $\tau(x_j)$ is the directly calculated value of the position and $\tau_R(x_j)$ is the predicted value of the position, calculated by using the linear regression method. The power equivalent width is $\sigma = \sum_{i=1}^{N}(|U(x,t_i)|^2 dt/\eta^2)$. $U(x,\omega) = \mathrm{FFT}[U(x,t)]$ is the spectral amplitude received by using the fast-Fourier transformation.

III. ODE SYSTEM

If we consider giving the terms in the right side of Eq. (1) small values, we can find its solution as a perturbed soliton solution of the nonlinear Schrödinger equation (NLSE) in the form [56]

$$U(x,t) = \eta(x)\mathrm{sech}\{\eta(x)[t-\tau(x)]\}\exp\{-ik(x)t + i\sigma(x)\}, \quad (2)$$

where $\eta(x)$ and $k(x)$ are, respectively, the soliton amplitude and frequency. Besides, $d[\tau(x)]/dx = -k$, and $d[\sigma(x)]/dx = (1/2)(\eta^2 - \kappa^2)$ are the pulse position and pulse phase.

Using the first two preserved quantities of the NLSE, namely, the total energy and the momentum (or the mean frequency) [16,21,22,24], i.e.,

$$C_1 = \int_{-\infty}^{+\infty} |U(x,t)|^2\, dt,$$

$$C_2 = \frac{i}{2}\int_{-\infty}^{+\infty}\left[U(x,t)\frac{\partial U^*(x,t)}{\partial t} - U^*(x,t)\frac{\partial U(x,t)}{\partial t}\right]dt,$$

the following ODE system, describing the evolution and frequency of the soliton amplitude, has been derived [39,40,44,45]:

$$\frac{d\eta}{dx} = 2\delta\eta + \frac{2}{3}(2\varepsilon-\beta)\eta^3 - 2\beta\eta k^2 + \frac{16}{15}\mu\eta^5,$$
$$\frac{dk}{dx} = -\frac{4}{3}\beta\eta^2 k - \frac{8}{15}\gamma\eta^4. \tag{3}$$

We should note that *Mathematica 8.0* [57] has been used for the numerical calculation of System (3). Involving the notations,

$$c_1 = 2\delta,\quad c_2 = \tfrac{2}{3}(2\varepsilon-\beta),\quad c_3 = -2\beta,$$
$$c_4 = \tfrac{16}{15}\mu,\quad c_5 = -\tfrac{4}{3}\beta,\quad c_6 = -\tfrac{8}{15}\gamma,$$

in System (3) we have

$$\frac{d\eta}{dx} = c_1\eta + c_2\eta^3 + c_3\eta k^2 + c_4\eta^5 = P(\eta,k),$$
$$\frac{dk}{dx} = c_5\eta^2 k + c_6\eta^4 = Q(\eta,k). \tag{4}$$

To obtain the fixed points we rewrite System (4) in the following way: we multiply the first equation with η taking into account that $\eta\frac{d\eta}{dx} = \frac{1}{2}\frac{d\eta^2}{dx}$ and System (4) takes the following form:

$$\frac{d\eta^2}{dx} = 2c_1\eta^2 + 2c_2\eta^4 + 2c_3\eta^2k^2 + 2c_4\eta^6,$$
$$\frac{dk}{dx} = c_5\eta^2 k + c_6\eta^4.$$

Next, we introduce notation $\xi = \eta^2$, $\xi > 0$, $\eta = \pm\sqrt{\xi}$. Thus, the last system takes the form

$$\frac{d\xi}{dx} = \xi(2c_1 + 2c_2\xi + 2c_3k^2 + 2c_4\xi^2),$$
$$\frac{dk}{dx} = \xi(c_5k + c_6\xi). \tag{5}$$

It is seen that the first fixed point is $\xi = 0$ and k is arbitrary, which can be shown as $(\eta_0, k_0) = (0, k)$. The other fixed points can be found in the following system:

$$2c_1 + 2c_2\xi + 2c_3k^2 + 2c_4\xi^2 = 0,$$
$$c_5k + c_6\xi = 0.$$

As can be seen, the second equation of the system above gives $k = -(c_6/c_5)\xi$. Substituting this expression in the first equation, we get the quadratic equation $A\xi^2 + \xi + B = 0$, where

$$A = \frac{c_4}{c_2} + \frac{c_3}{c_2}\frac{c_6^2}{c_5^2},\quad B = \frac{c_1}{c_2}.$$

The roots of this equation are $\xi_{1,2} = (-1 \pm \sqrt{1-4AB})/2A$. To have real roots, the following conditions should be satisfied: $1-4AB \geqslant 0$, $AB \leqslant 1/4$, and $\xi_{1,2} > 0$. Needless to say, the fixed points in the form (ξ, k) are easily transformed into the original coordinates (η, k). The possible variants for the fixed points depending on A and B are given in the Appendix.

IV. BIFURCATION ANALYSIS OF THE ODE SYSTEM (4)

Our bifurcation analysis of System (4) follows the approach described in [47]. To facilitate the comparison of our analysis with that of [47], we use similar notations.

A linearization of System (4) at its fixed points is made by applying the Taylor series expansion in the neighborhood of these points on the right side of the system. Let us assume that $(\bar\eta, \bar k)$ is an arbitrary fixed point of System (4); i.e., $P(\bar\eta,\bar k) = 0$, $Q(\bar\eta,\bar k) = 0$. Then we change the variables (η, k) with new ones (u, v) in the following way: $u = \eta-\bar\eta$, $v = k-\bar k$, $\dot\eta = \dot u$, $\dot k = \dot v$. The beginning of the new coordinate system will be in a fixed point, or the fixed point of the new coordinate system becomes $(0, 0)$. The coefficients in the Taylor series are calculated with the coordinate of the original fixed point $(\bar\eta, \bar k)$. In the new variables (local coordinates), System (4) takes the following form [47]:

$$\frac{du}{dx} = au + bv + P_2(u,v) + P_3(u,v) + \cdots = F(u,v),$$
$$\frac{dv}{dx} = cu + dv + Q_2(u,v) + Q_3(u,v) + \cdots = G(u,v). \tag{6}$$

Here $a = P'_\eta(\bar\eta,\bar k)$, $b = P'_k(\bar\eta,\bar k)$, $c = Q'_\eta(\bar\eta,\bar k)$, $d = Q'_k(\bar\eta,\bar k)$. The matrix $A = (\begin{smallmatrix} a & b\\ c & d\end{smallmatrix})$ describes the linear part on the right side of System (6). The characteristic equation of A is

$$\lambda^2 - \sigma\lambda + \Delta = 0, \tag{7}$$

where $\sigma = \mathrm{tr}A = a + d$ and $\Delta = \det A = ad-bc$.

The eigenvalues of the matrix A or the roots of the characteristic Eq. (7) can be presented as

$$\lambda_{1,2} = \tfrac{1}{2}[\sigma \pm \sqrt{\sigma^2 - 4\Delta}] = \tfrac{1}{2}[\mathrm{tr}A \pm \sqrt{(\mathrm{tr}A)^2 - 4\det A}]. \tag{8}$$

$P_i(u, v)$ and $Q_i(u, v)$, where $i = 2, 3$ are given by

$$P_2(u,v) = a_{20}u^2 + a_{11}uv + a_{02}v^2,$$
$$Q_2(u,v) = b_{20}u^2 + b_{11}uv + b_{02}v^2,$$
$$P_3(u,v) = a_{30}u^3 + a_{21}u^2v + a_{12}uv^2 + a_{03}v^3,$$
$$Q_3(u,v) = b_{30}u^3 + b_{21}u^2v + b_{12}uv^2 + b_{03}v^3.$$

The quantities a, b, c, d, a_{ij}, and b_{ij} are calulated as follows:

$$a = c_1 + 3c_2\bar\eta^2 + c_3\bar k^2 + 5c_4\bar\eta^4,\quad b = 2c_3\bar\eta\bar k,$$
$$a_{20} = 3c_2\bar\eta + 10c_4\bar\eta^3,\quad a_{11} = 2c_3\bar k,\quad a_{02} = c_3\bar\eta,$$
$$a_{30} = c_2 + 10c_4\bar\eta^2,\quad a_{21} = 0,\quad a_{12} = c_3,\quad a_{03} = 0,$$
$$c = 2c_5\bar\eta\bar k + 4c_6\bar\eta^3,\quad d = c_5\bar\eta^2,$$

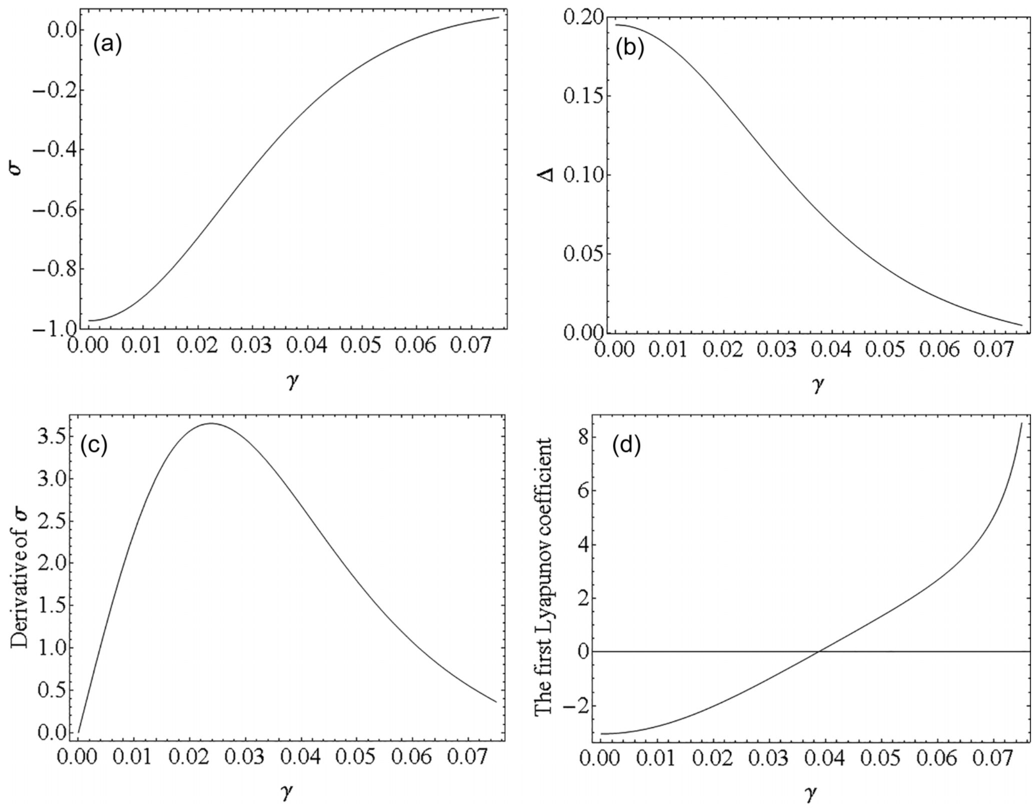

FIG. 1. Values of (a) $\sigma(\gamma)$, (b) $\Delta(\gamma)$, (c) $\frac{d\sigma}{d\gamma}(\gamma)$, and (d) $L_1(\gamma)$, as functions of parameter γ.

$$b_{20} = c_5\bar{k} + 6c_6\bar{\eta}^2, \quad b_{11} = 2c_5\bar{\eta}, \quad b_{02} = 0,$$
$$b_{30} = 4c_6\bar{\eta}, \quad b_{21} = c_5, \quad b_{12} = 0, \quad b_{03} = 0.$$

Therefore System (6) is completely determined. Point $(u_0, v_0) = (0, 0)$ is a fixed point for System (6); i.e., $F(0, 0) = 0$, $G(0, 0) = 0$. The Routh-Hurwitz conditions for stability of the fixed point (0, 0) are [47] $\sigma = a + d < 0$, $\Delta = ad - bc > 0$.

System (3) depends on a large number of parameters δ, β, ε, γ, μ having a different range of variation. In the further analysis, we focus our attention on parameter γ, which is related to the effect of IRS. In other words, γ is regarded as a bifurcation (critical) parameter, while the others, δ, β, ε, μ, are fixed. Hence, all the introduced quantities and coefficients into (6) and (7) are considered to be functions of γ. For example, $\sigma(\gamma) = a(\gamma) + d(\gamma)$, $\Delta(\gamma) = a(\gamma)d(\gamma) - b(\gamma)c(\gamma)$. (The notation $R(\gamma) = \sigma(\gamma)$ is also used [47].)

From the Poincaré-Andronov-Hopf bifurcation theory [46–49] it follows that System (3) possesses a limit cycle (periodic orbit) only in the case when parameter γ takes the critical value of the bifurcation parameter γ_b, for which the following nonhyperbolicity condition (conjugate pair of imaginary eigenvalues) and transversality condition (the eigenvalues cross the imaginary axis with nonzero speed) are satisfied; i.e.,

$$\sigma(\gamma_b) = \mathrm{tr}A(\gamma_b) = R(\gamma_b) = 0,$$
$$\Delta(\gamma_b) = \det A(\gamma_b) > 0, \quad (\mathrm{tr}A)^2 - 4\det A < 0, \tag{9a}$$

and

$$\frac{d\sigma(\gamma_b)}{d\gamma} = \frac{dR(\gamma_b)}{d\gamma} \neq 0. \tag{9b}$$

In this case the eigenvalues of matrix A are imaginary, $\lambda_{1,2} = \pm i\lambda_{\mathrm{im}}$. The period of the periodic motion related to the PAH bifurcation is described by

$$T = 2\pi/\lambda_{\mathrm{im}}. \tag{9c}$$

According to [46,47], the first Lyapunov coefficient (number) is

$$\begin{aligned} L_1 = &-\left(\frac{\pi}{4b\omega^3}\right)\big\{\big[ac\big(a_{11}^2 + a_{11}b_{02} + a_{02}b_{11}\big) \\ &+ ab\big(b_{11}^2 + b_{11}a_{20} + b_{20}a_{11}\big) + c^2(a_{11}a_{02} + 2a_{02}b_{02}) \\ &- 2ac\big(b_{02}^2 - a_{20}a_{02}\big) - 2ab\big(a_{20}^2 - b_{20}b_{02}\big) \\ &- b^2(2a_{20}b_{20} + b_{11}b_{20}) + (bc - 2a^2)(b_{11}b_{02} - a_{11}a_{20}) \\ &- (a^2 + bc)[3(cb_{03} - ba_{30}) \\ &+ 2a(a_{21} + b_{21}) + (ca_{12} - b_{21}b)]\big]\big\}, \end{aligned} \tag{10}$$

where $\omega^2 = (ad - bc) > 0$. If $L_1 \neq 0$, then the origin is a weak focus of multiplicity 1. It is stable if $L_1 < 0$ [a soft supercritical reversible Poincaré-Andronov-Hopf bifurcation (PAHB) occurs)] and unstable if $L_1 > 0$ (a hard subcritical nonreversible PAHB occurs) [46–50,58,59]. In our case $L_1 = L_1(\gamma)$.

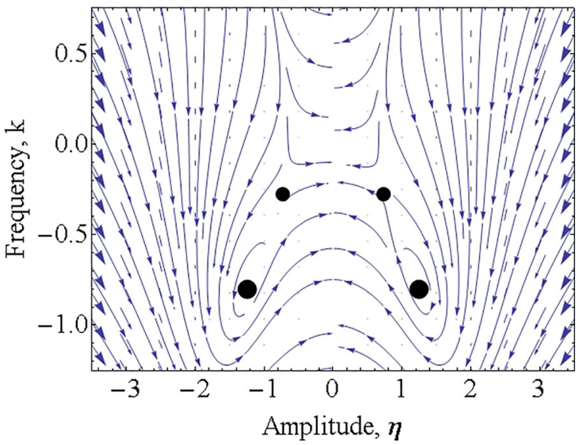

FIG. 2. Phase portrait of System (3) for $\delta = -0.02$, $\beta = 0.05$, $\varepsilon = 0.1$, $\mu = -0.02$, and $\gamma = \gamma_b = 0.0640833$.

V. STUDY OF THE SUBCRITICAL PAHB DUE TO THE INTRAPULSE RAMAN SCATTERING

It is believed that if $\delta < 0$, $\beta > 0$ then the background instability is avoided [16,60]. We fix the parameters $\delta = -0.02$, $\beta = 0.05$, $\varepsilon = 0.1$, $\mu = -0.02$, and use different values for γ.

Our aim in this section is to perform a detailed investigation of the appearance of subcritical PAHB in the CCQGLE in the presence of IRS. In order to identify this bifurcation and to study it, we apply our model given by Eq. (3). As has already been mentioned, this dynamic model has been derived earlier and applied in the analysis of the solutions of CCQGLE in [39,40,44,45]. However, we will focus our attention on a detailed qualitative and numerical study of the appearance (existence) of the periodic solutions of the CCQGLE. We will proceed in the following way. First, we will present the results from the phase and bifurcation analysis of System (3). After that we will present the corresponding results from the numerical solution of the CCQGLE. Finally, our numerical findings will be compared qualitatively with those from step 1. Hence, it will be possible for us (i) to discover some properties of the CCQGLE and (ii) to estimate the usefulness of System (3) in the analysis of the periodic solutions of the CCQGLE, which are connected with PAHB.

It is well known that in the case of a subcritical PAHB (i.e., when $L_1 > 0$), locally, we have a branch of unstable periodic solutions (limit cycles) and a branch of stable fixed points (focal points) on one side of the bifurcation and a branch of unstable fixed points (focal points) on the other side of the bifurcation point [46–50]. Here, as a result of our study, it will be demonstrated that the first part of this scenario corresponds to smaller values of γ denoted as γ^* ($\gamma^* < \gamma_b$). The boundary between the first two bifurcation branches is connected with γ_b—the bifurcation value of γ. Notice that the branch with the unstable focal point will be related to γ^{**} ($\gamma_b < \gamma^{**}$).

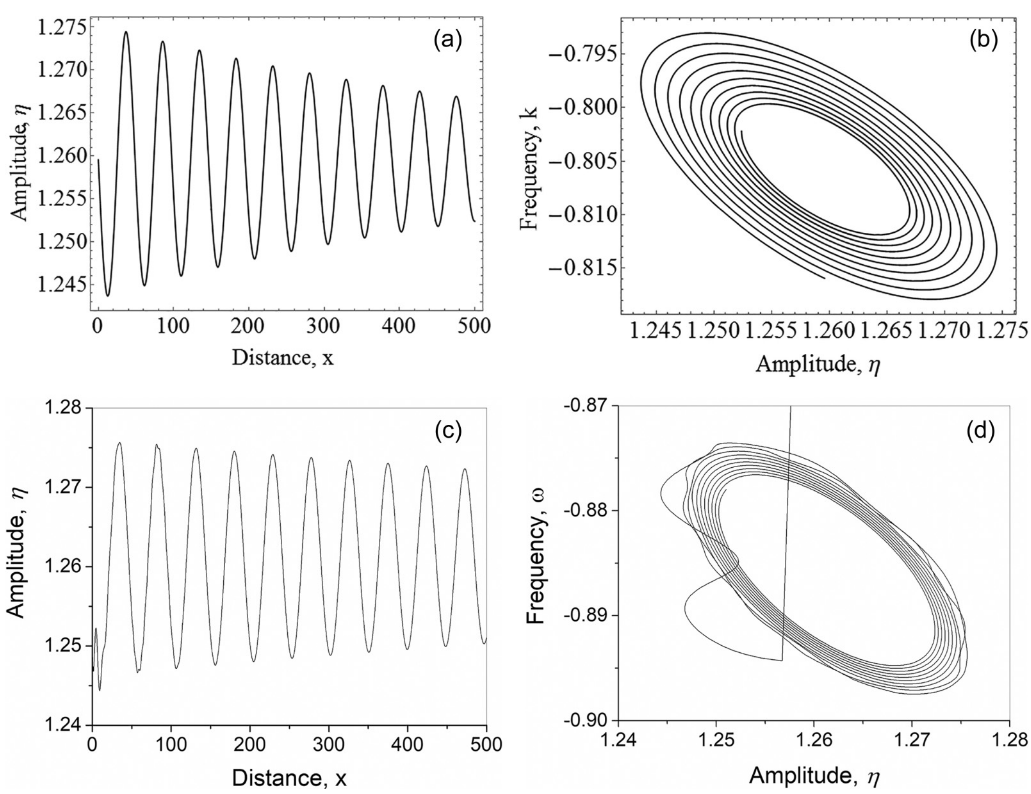

FIG. 3. Results obtained by the numerical solution of dynamic model (3) and Eq. (1) for distance $x_{\max} = 500$ and intial condition (1.259 56, −0.815 943), when the values of the parameters are $\delta = -0.02$, $\beta = 0.05$, $\varepsilon = 0.1$, $\mu = -0.02$, and $\gamma = 0.0635$. (a) Evolution of the amplitude of the numerical solution $\eta(x)$ according to Eq. (3). (b) Parametric plot (phase portrait) of the pulse amplitude $\eta(x)$ and frequency $k(x)$ according to Eq. (3). (c) Evolution of the amplitude of the numerical solution $\eta(x)$ according to Eq. (1) with initial condition $\eta_0 = 1.259\,56$ and $\omega_0 = -0.815\,943$ for distance $x_{\max} = 500$. (d) Parametric plot of the numerical solution $\eta(x)$ and frequency $\omega(x)$ according to Eq. (1).

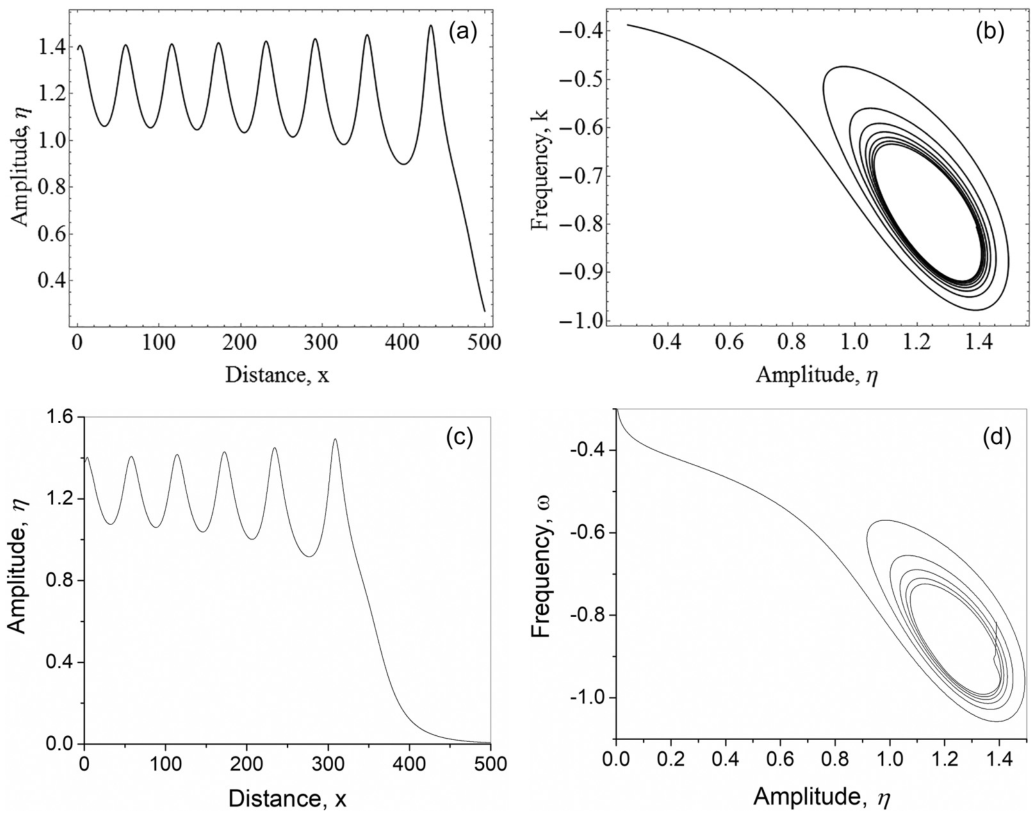

FIG. 4. Results obtained by the numerical solution of dynamic model (3) and Eq. (1) for distance $x_{\max} = 500$ and initial condition $(1.39,\ -0.805\,943)$ when the values of the parameters are $\delta = -0.02$, $\beta = 0.05$, $\varepsilon = 0.1$, $\mu = -0.02$, and $\gamma = 0.0635$. (a) Evolution of the amplitude of the numerical solution according to Eq. (3). (b) Parametric plot of the pulse amplitude $\eta(x)$ and frequency $k(x)$ according to Eq. (3). (c) Evolution of the amplitude of the numerical solution $\eta(x)$ according to Eq. (1), with initial condition $\eta_0 = 1.39$ and $\omega_0 = -0.805\,943$ for distance $x_{\max} = 500$. (d) Parametric plot of the numerical solution $\eta(x)$ and frequency $\omega(x)$ according to Eq. (1).

For the above-mentioned values of parameters δ, β, ε, and μ, according to [44,45], it is known that for System (3) when $\gamma = \gamma_b = 0.064\,083\,3$ (see also Fig. 1) a PAHB appears as a fixed point with coordinates $(1.25,\ -0.801\,043)$. To portray the above-described subcritical PAHB, we obtain acceptable values for $\gamma^* < \gamma_b$ and $\gamma_b < \gamma^{**}$, so that the following conditions are satisfied [47]: $\gamma^* : \sigma < 0,\ L_1 > 0,\ \gamma_b : \sigma = 0,\ L_1 > 0,\ \gamma^{**} : \sigma > 0,\ L_1 > 0$. To demonstrate this bifurcation behavior, the corresponding dependences of $\sigma,\ \Delta,\ \frac{d\sigma}{d\gamma}$ and L_1 by γ are shown in Fig. 1.

Varying the effect of IRS, γ, three observations could be made in Fig. 1. First, Figs. 1(a), 1(c), and 1(d) numerically prove the fact that $\gamma_b = \gamma = 0.064\,083\,3$ is a bifurcation value of γ, as $\sigma(\gamma_b) = 0$, $L_1(\gamma_b) > 0$, and $\frac{d\sigma}{d\gamma}(\gamma_b) > 0$. Second, it shows that γ^* can be chosen as $\gamma^* = 0.0635 < \gamma_b$, because $\sigma(\gamma^*) < 0,\ L_1(\gamma^*) > 0$. Third, we see that γ^{**} could be chosen as $\gamma^{**} = 0.0645 > \gamma_b$, because $\sigma(\gamma^{**}) > 0,\ L_1(\gamma^{**}) > 0$. Therefore, to describe the subcritical PAHB we will use the following values of γ: $\gamma^* = 0.0635 < \gamma_b$ to characterize the branch of unstable periodic solutions and the branch of stable focal points on the other side of the bifurcation; $\gamma_b = 0.064\,083\,3$ is used to describe the boundary between the two branches of bifurcation; and finally, $\gamma^{**} = 0.0645 > \gamma_b$ is used for the branch of the unstable focal point on the other side of the bifurcation point.

Now it is completely clear that the value $\gamma_b = \gamma = 0.064\,083\,3$ which we found earlier (when $\delta = -0.02$, $\beta = 0.05$, $\varepsilon = 0.1$, $\mu = -0.02$) [44,45], is a boundary between the two branches as the respective fixed point is a multiple focus of multiplicity 1. Moreover, for these values of the parameters, in accordance with the Appendix (see case 3), System (3) has five fixed points: $(\eta_0, k_0) = (0,\ \text{arbitrary})$, $(\eta_1, k_1) = (0.733\,235,\ -0.275\,625)$, $(\eta_2, k_1) = (-0.733\,235,\ -0.275\,625)$, $(\eta_3, k_2) = (1.25,\ -0.801\,043)$, $(\eta_4, k_2) = (-1.25,\ -0.801\,043)$. The phase portrait with these fixed points is shown in Fig. 2.

As can be seen from Fig. 2, the line $(\eta_0, k_0) = (0,\ \text{arbitrary})$ is an attractor, so the fixed points (a straight line) are all nonsimple [61]. Our investigation has shown (see below) that the fixed points (presented through small black points) $(\eta_1, k_1) = (0.733\,235,\ -0.275\,625)$, and $(\eta_2, k_1) = (-0.733\,235,\ -0.275\,625)$ are saddles, while the fixed points (shown through large black points) $(\eta_3, k_2) = (1.25,\ -0.801\,043)$ and $(\eta_4, k_2) = (-1.25,\ -0.801\,043)$ are foci. In the following paragraphs, our attention will be focused both on fixed points: $(\eta_3, k_2) = (1.25,\ -0.801\,043)$ and $(\eta_1, k_1) = (0.733\,235,\ -0.275\,625)$. Notice that the other two nonzero fixed points have similar properties. First, we will consider fixed point (η_3, k_2).

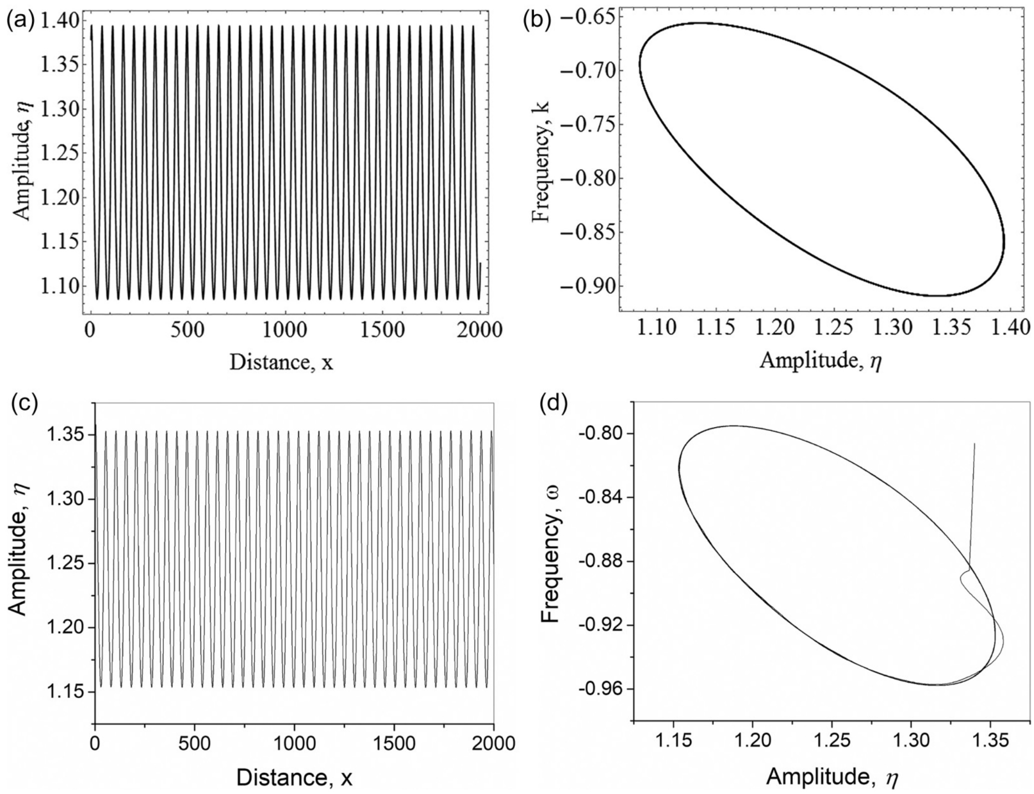

FIG. 5. Results obtained by the numerical solution of dynamic model (3) and Eq. (1) for distance $x_{\max} = 2000$ when the values of the parameters are $\delta = -0.02$, $\beta = 0.05$, $\varepsilon = 0.1$, $\mu = -0.02$, and $\gamma = 0.0635$. (a) Evolution of the amplitude of the numerical solution $\eta(x)$ according to Eq. (3) with initial conditions (1.378 344 6, −0.805 943). (b) Parametric plot of the pulse amplitude $\eta(x)$ and frequency $k(x)$ according to Eq. (3). (c) Evolution of the amplitude of the numerical solution $\eta(x)$ according to Eq. (1), with initial condition $\eta_0 = 1.34$ and $\omega_0 = -0.805\,943$. (d) Parametric plot of the numerical solution $\eta(x)$ and frequency $\omega(x)$ according to Eq. (1).

A. Below the critical bifurcation value $\gamma^* = 0.0635 < \gamma_b$

Here we study the branch of unstable periodic solutions and the branch of stable focal points on the left side of the bifurcation, i.e., $\gamma^* = 0.0635 < \gamma_b$. For $\gamma^* = 0.0635$, the corresponding fixed point coordinates are $(\eta_3, k_2) = (1.259\,56,\ -0.805\,943)$. On the other hand, the quantities which present interest for us are $\sigma = -0.003\,249\,51 < 0$, $\Delta = 0.016\,637\,2 > 0$, $\sigma^2 - 4\Delta = -0.066\,538\,2 < 0$, $\frac{d\sigma(\gamma_b)}{d\gamma} = 0.865\,515$, $\lambda_{1,2} = -0.001\,624\,75 \pm 0.128\,975i$, and $L_1 = 3.289\,65$. It is clearly seen that the real parts of the eigenvalues are different from zero and below zero (negative). Therefore, this fixed point is a stable focus. The numerical solution of System (3) with initial condition $(\eta_3, k_2) = (1.259\,56,\ -0.805\,943)$ for distances of $x_{\max} = 500$, which gives no changes in the amplitude and frequency, is in good agreement with this qualitative result. However, if we slightly change the frequency (or use it as the initial condition) in the form (1.259 56, −0.815 943), we get results that are typical for the stable focus—see Figs. 3(a) and 3(b).

Figures 3(a) and 3(b) demonstrate the expected damping oscillations of the amplitude toward the stable focus. It should be mentioned that the reduction is very slow due to the small values of the real eigenvalues. In particular, analogous results are obtained by the numerical solution of Eq. (1)—see Figs. 3(c) and 3(d). If we compare Fig. 3(a) with Fig. 3(c) and Fig. 3(b) with Fig. 3(d), we can observe a close correspondence, so we may conclude that the predicted behavior (stable focus) in System (3) appears in the perturbed CCGLE, too.

Outside the unstable periodic solutions in this branch we expect that the plotting point on the phase portrait will continuously increase its amplitude. Our numerical study of System (3) has confirmed this expectation. An example of this behavior is shown in Figs. 4(a) and 4(b), which present our results from the numerical solution of System (3) with initial condition (1.39, −0.805 943) for distances of $x_{\max} = 500$.

It is clearly seen that Figs. 4(a) and 4(b) confirm the expected behavior of the increasing oscillations. Analogous results obtained by the numerical solution of Eq. (1) are shown in Figs. 4(c) and 4(d). A comparison between Figs. 4(a) and 4(c) as well as Figs. 4(b) and 4(d) shows a good qualitative correspondence between those results. Moreover, up to a distance of $x \approx 300$ we have good quantitative agreement. Again, we may conclude that the predicted behavior of System (3) also appears in the perturbed CCGLE.

Next, we have tried to identify an unstable limit cycle of System (3) by using its numerical solution. Having in mind the results shown in Figs. 3(a) and 3(b) and Figs. 4(a) and 4(b) we have changed the initial amplitude in the region $\eta_0 \subseteq [1.259\,56,\ 1.39]$, keeping the frequency value unchanged. An example of such a calculation with initial condition (1.378 344 6, −0.805 943) and distance $x_{\max} = 2000$ is shown in Figs. 5(a) and 5(b).

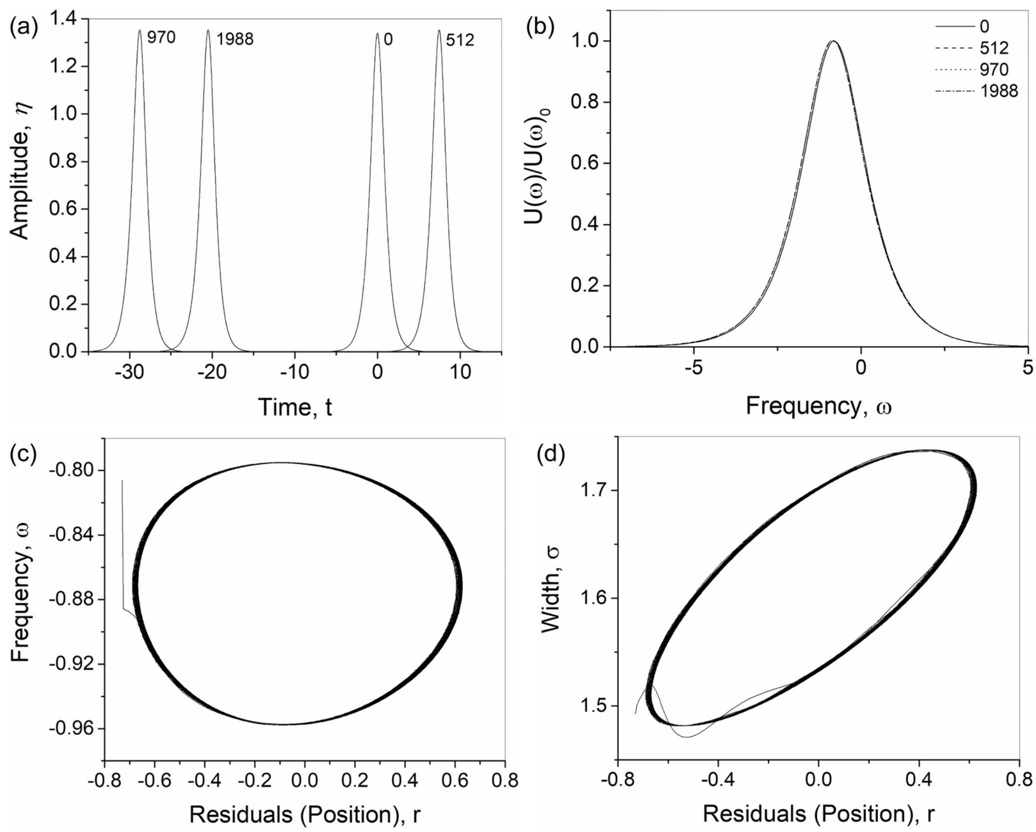

FIG. 6. Numerical properties of the pulse propagating in the condition of PAHB according to Eq. (1) with $\delta = -0.02$, $\beta = 0.05$, $\varepsilon = 0.1$, $\mu = -0.02$, and $\gamma = 0.0635$ with $x_{\max} = 2000$ and initial conditions $(1.34,\ -0.805\,94)$. The numerical parameters are step size 1/2000, sampling rate 2^{15}, and time resolution 0.002 44. (a) represents the shape of the propagating pulse at different distances $x = 0,\ 512,\ 970,\ 1988$. (b) presents a comparison between the spectrum of the pulses at the same distance. In principle, the parametric plots in (c,d) show the correlation between the frequency and position evolution of the pulse width with changing the distance and the correlation between the pulse width and the position with changing the distance. All results presented in this figure have been obtained by using Agrawal's split-step Fourier method with one iteration.

As can be seen from Figs. 5(a) and 5(b) for the chosen initial condition and distance $x_{\max} = 2000$ we have obtained a periodicity typical for a limit cycle. The period of fluctuations of PAHB according to Eq. (9c) is $T \approx 50$. In the simulation shown in Fig. 5(c), the period of oscillations from the numerical solution of Eq. (1) is $T_{\text{num}} \approx 50$. Both results agree quite well. In fact, the period of the PAHB calculated according to Eq. (9c) is applicable for all our results presented in Figs. 3–6 and 8–10.

Interestingly, the behavior of the periodic soution in Fig. 5(a) could be observed at much larger distances than $x = 2000$, if, however, we add more digits after the decimal point in the amplitude of the initial condition. As the bifurcation value $\gamma = \gamma_b = 0.064\,083\,3$ is also defined with some accuracy, we have not proceeded further in this direction.

It has already been mentioned that our main aim in this study is to find a limit cycle in Eq. (1). Thus, using the parameters identified in the bifurcation analysis of System (3), namely, $\delta = -0.02$, $\beta = 0.05$, $\varepsilon = 0.1$, $\mu = -0.02$, and $\gamma = \gamma_b = 0.0635$ [used to achieve the results in Figs. 5(a) and 5(b)], we obtain the numerical solution of Eq. (1) for slightly different initial conditions from $(1.378\,344\,6,\ -0.805\,943)$. Figures 5(c) and 5(d) present an important result from these calculations. Using the same parameters [as those in Figs. 5(a) and 5(b)] but for different initial conditions given by $(1.34,\ -0.805\,94)$, we have observed periodic behavior of the pulse amplitude at a very long distance $x_{\max} = 2000$ of the direct numerical solution of Eq. (1). We interpret these results as a numerical observation of the limit cycle of the CCGLE perturbed with IRS.

If we compare Fig. 5(a) with Fig. 5(c) and Fig. 5(b) with Fig. 5(d), we can see a remarkable correspondence. In this case we introduce a measure for the amplitude deviation of the numerical solution of Eq. (1): the amplitude value of 1.34 from the numerical solution of the equation becomes 1.38 identified by the bifurcation theory, which shows a deviation of approximately 3%. Therefore we can say that by employing the bifurcation analysis, we have successfully predicted a periodic solution (limit cycle) of the CCQGLE in the presence of IRS! Moreover, when comparing the forms and sizes of the limit cycle in Figs. 5(b) and 5(d) we can see a well-expressed qualitative similarity. Based on these facts, we may state that the most important result from this study is the prediction of the limit cycle by the bifurcation theory and the identification of a similar limit cycle in the CCQGLE in the presence of IRS.

The numerical results presented in Figs. 5(c) and 5(d) are obtained by the numerical solution of Eq. (1) with Agrawal's split-step Fourier method with one and two iterations.

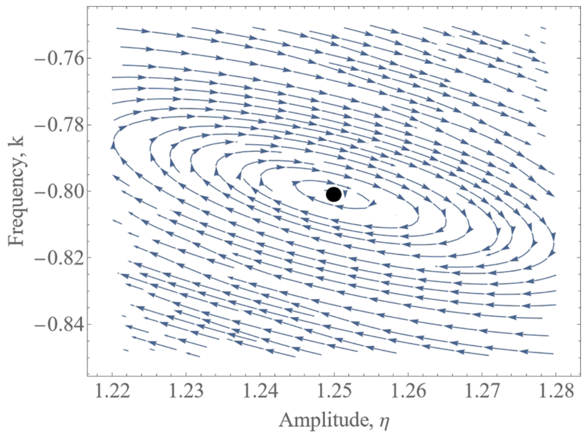

FIG. 7. Phase portrait of System (3) in the neighborhood of fixed point $(\eta_3, k_2) = (1.25,\ -0.801\,043)$ for $\delta = -0.02$, $\beta = 0.05$, $\varepsilon = 0.1$, $\mu = -0.02$, and $\gamma = \gamma_b = 0.064\,083\,3$.

Now let us discuss the properties of the propagating pulse in the conditions of PAHB. In Fig. 6 we take a closer look at the evolutions of the following properties of the pulse: (a) peak amplitude, (b) temporal shape, (c) frequency spectrum, (d) width, and (e) position.

Figures 6(a) and 6(b) show the nice saving of the temporal shape and frequency spectrum of the propagating pulse at all distances. Furthermore, the periodic changes of the frequency, width, and position of the pulse are clearly seen in Figs. 6(c) and 6(d).

B. At the critical bifurcation value $\gamma = \gamma_b = 0.064\,083\,3$

Here the boundary between the two branches of bifurcation will be studied. The boundary is characterized by the bifurcation value $\gamma = \gamma_b = 0.064\,083\,3$. This value leads to a fixed point $(\eta_3, k_2) = (1.25,\ -0.801\,041)$. At the same time, the quantities which present interest for us are $\sigma = 1.14 \times 10^{-7} \sim 0$, $\Delta = 0.0159 > 0$, $\sigma^2 - 4\Delta = -0.063\,541\,6 < 0$, $\frac{d\sigma(\gamma_b)}{d\gamma} = 0.8344$, $\lambda_{1,2} = 5.704\,02 \times 10^{-8} \pm 0.126\,04i$, and $L_1 = 3.405\,18 > 0$. Having in mind the accuracy with which the bifurcation value of γ ($\gamma_b = 0.064\,083\,3$) has been calculated, we can assume that $\sigma \sim 0$ and the eigenvalues of the matrix A are purely imaginary; i.e., $\lambda_{1,2} \sim \pm 0.126\,04i$. Additionally, the derivative $\frac{d\sigma(\gamma_b)}{d\gamma} = 0.8344$ is different from zero. Therefore we can conclude that all conditions required for the existence of PAHB given by Eqs. (9a) and (9b) and Eq. (10) are satisfied. According to [46,47], this fixed point is multiple foci of multiplicity 1. See Fig. 7.

Following the above discussion, the corresponding numerical solution of System (3) with the initial condition $(\eta_3, k_2) = (1.25,\ -0.801\,043)$ gives us the results shown in Fig. 8.

The reason for the usage of relative amplitudes and frequencies is the very slight change in the amplitude and frequency. As can be seen from Figs. 8(a) and 8(b), the movement of the plotting point is practically close to the

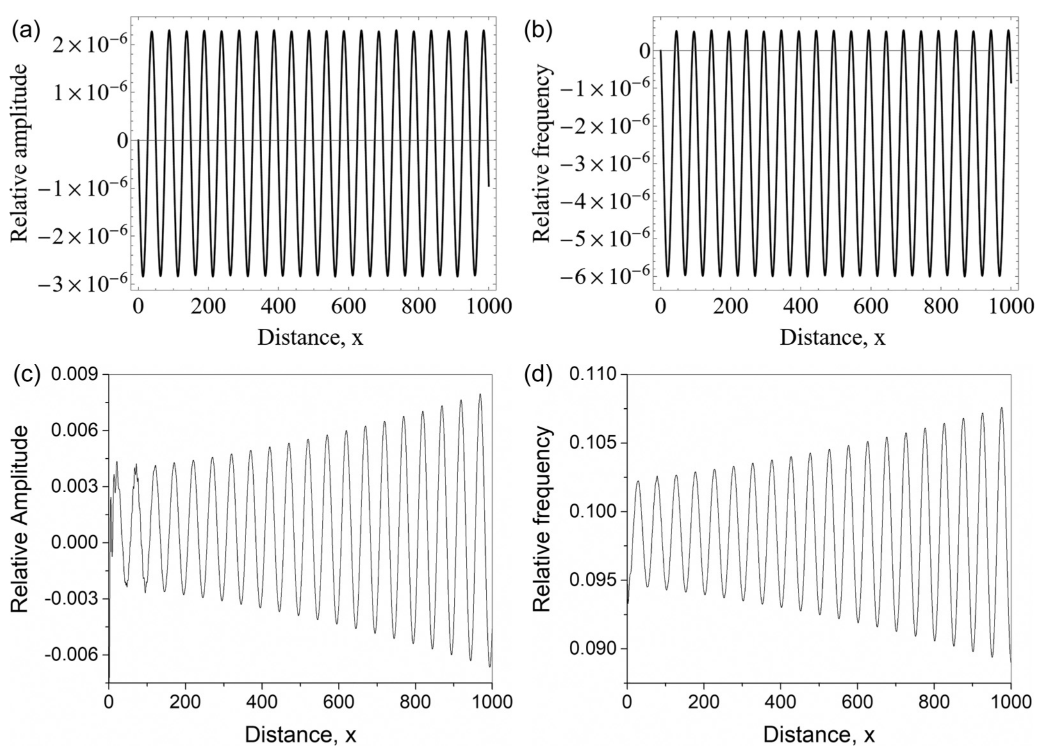

FIG. 8. Results obtained by the numerical solution of dynamic model (3) and Eq. (1) with parameters $\delta = -0.02$, $\beta = 0.05$, $\varepsilon = 0.1$, $\mu = -0.02$, and $\gamma = \gamma_b = 0.064\,083\,3$ for distance $x_{\max} = 1000$. (a) Evolution of the relative amplitude of the numerical solution $[\eta(x) - \eta_3]/\eta_3$ according to Eq. (3) and initial conditions $(\eta_3, k_2) = (1.25,\ -0.801\,043)$. (b) Evolution of the relative frequency of the numerical solution $[k(x) - k_2]/k_2$ according to Eq. (3) for the same parameters as in (a). (c) Evolution of the relative amplitude of the numerical solution $[\eta(x) - \eta_0]/\eta_0$ according to Eq. (1) with initial condition $\eta_0 = 1.25$ and $\omega_0 = -0.801\,043$. (d) Evolution of the relative frequency of the numerical solution $[\omega(x) - \omega_0]/\omega_0$ according to Eq. (1) for the same parameters as in (c).

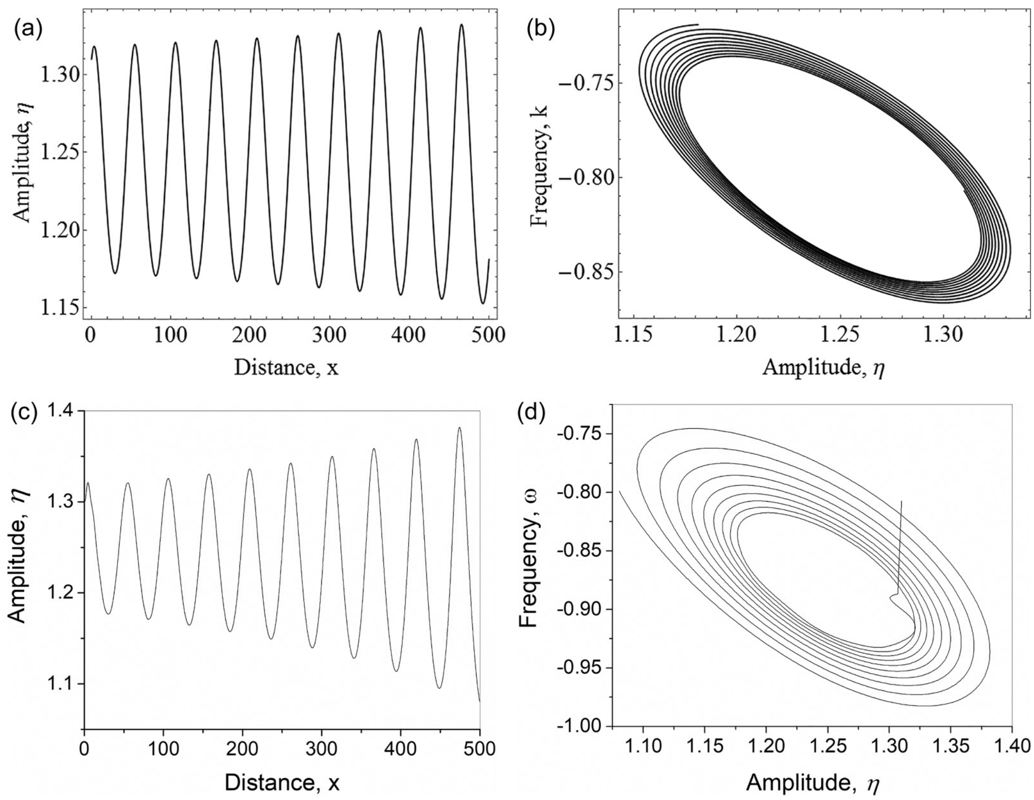

FIG. 9. Results obtained by the numerical solution of dynamic model (3) and Eq. (1) with parameters $\delta = -0.02$, $\beta = 0.05$, $\varepsilon = 0.1$, $\mu = -0.02$, and $\gamma = \gamma_b = 0.064\,083\,3$ for distance $x_{\max} = 500$. (a) Evolution of the amplitude of the numerical solution $\eta(x)$ according to Eq. (3) and initial conditions $(1.31,\ -0.807\,443)$. (b) Parametric plot of the pulse amplitude $\eta(x)$ and frequency $k(x)$ according to Eq. (3) for the same parameters as in (a). (c) Evolution of the amplitude of the numerical solution $\eta(x)$ according to Eq. (1) with initial condition $\eta_0 = 1.31$ and $\omega_0 = -0.807\,443$. (d) Parametric plot of the numerical solution $\eta(x)$ and frequency $\omega(x)$ according to Eq. (1).

periodic solution with a very small amplitude near the bifurcation point. At the bifurcation value of $\gamma = \gamma_b = 0.064\,083\,3$, the focus is nonlinearly unstable [49]. Here the nonlinearity means that the rate of the movement of the plotting point is no longer exponential. Sometimes it is called "weakly attracting" or "repelling focus" [49]. We should note here that for System (3) this behavior at the bifurcation point has been reported in [44]. The results from the numerical simulations of Eq. (1) with the same parameters and initial conditions are presented in Figs. 8(c) and 8(d). A comparison between Figs. 8(a) and 8(c) as well as between Figs. 8(b) and 8(d) shows well-expressed differences. The common feature between Figs. 8(a) and 8(c) is their periodicity or, more precisely, the equal period of the fluctuations.

Having in mind the phase portrait of System (3) at the fixed point $(\eta_3, k_2) = (1.25, -0.801\,043)$ (see Fig. 7), we can predict that after a proper choice of plotting point (initial conditions), there will possibly appear periodically developing solutions with slowly increasing amplitude. This scenario is illustrated by the results of our numerical calculations of System (3) in Figs. 9(a) and 9(b).

As can be seen from Figs. 9(a) and 9(b) we get almost periodic solutions that do not depend on distance. These solutions are with relatively large fluctuations in amplitude. At larger distances (not presented here) the plotting point goes to the main attractor $(\eta_0, k_0) = (0,\ \text{arbitrary})$—see the phase portrait of System (3) in Fig. 1. Our predictions from Figs. 9(a) and 9(b) have been confirmed by the results from the numerical solution of Eq. (1). These results are presented in Figs. 9(c) and 9(d) and are in very good agreement with the results shown in Figs. 9(a) and 9(b).

Because of the slow change of the amplitude, we expect that such a regime could be of interest for some practical applications.

C. Above the critical bifurcation value $\gamma^{**} = 0.0645 > \gamma_b$

Here we will investigate the branch with an unstable focal point. It is related to γ^{**} $(\gamma_b < \gamma^{**})$. For $\gamma = \gamma^{**} = 0.0645$, the corresponding fixed point (η_3, k_2) becomes $(\eta_3, k_2) = (1.243\,15,\ -0.797\,443)$. In this case, the quantities which present interest for us are $\sigma = 0.002\,250\,88$, $\Delta = 0.015\,360\,2 > 0$, $\sigma^2 - 4\Delta = -0.061\,435\,7 < 0$, $\frac{d\sigma(\gamma_b)}{d\gamma} = 0.812\,621 \neq 0$, $L_1 = 3.490\,98 > 0$, and $\lambda_{1,2} = 0.001\,125\,44 \pm 0.123\,931i$. Since the real part of the eigenvalues is different from zero and above zero (positive), then this fixed point is an unstable focus.

The numerical solution of System (3) with initial condition $(1.243\,15,\ -0.797\,443)$ up to distances of $x_{\max} \sim 500$ does not show any change in the amplitude or frequency. If, however, we slightly change the frequency or use as the initial condition $(1.243\,15,\ -0.807\,443)$, we get the results presented in Figs. 10(a) and 10(b).

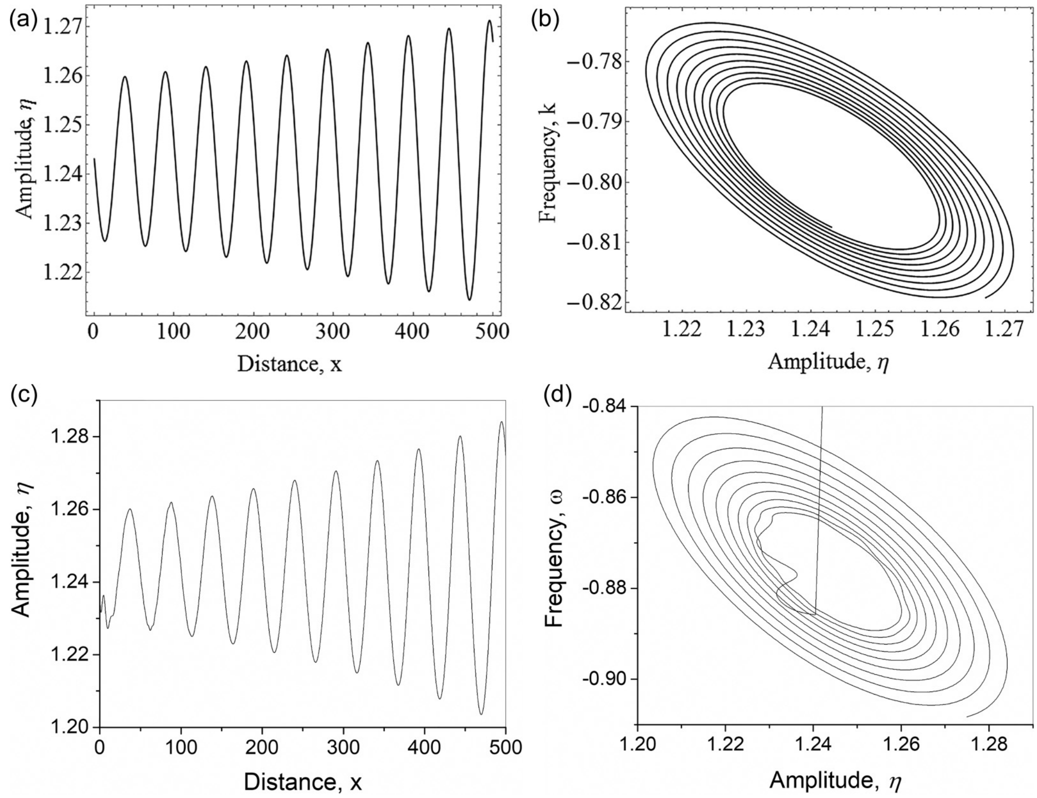

FIG. 10. Results obtained by the numerical solution of dynamic model (3) and Eq. (1) with parameters $\delta = -0.02$, $\beta = 0.05$, $\varepsilon = 0.1$, $\mu = -0.02$, and $\gamma = 0.0645$ for distance $x_{\max} = 500$. (a) Evolution of the amplitude of the numerical solution $\eta(x)$ according to Eq. (3) and initial conditions (1.243 15, −0.807 443). (b) Parametric plot of the pulse amplitude $\eta(x)$ and frequency $k(x)$ according to Eq. (3) for the same parameters as in (a). (c) Evolution of the amplitude of the numerical solution $\eta(x)$ according to Eq. (1) with initial condition $\eta_0 = 1.243\,15$ and $\omega_0 = -0.807\,443$. (d) Parametric plot of the numerical solution $\eta(x)$ and frequency $\omega(x)$ according to Eq. (1).

In Figs. 10(a) and 10(b) we can observe an expected behavior of the unstable focus. The results for the same parameters and initial conditions obtained by the numerical solution of Eq. (1) are presented in Figs. 10(c) and 10(d). If we compare Fig. 10(a) with Fig. 10(c) and Fig. 10(b) with Fig. 10(d), we will see again a very good correspondence, so we may conclude that the predicted unstable focus of System (3) (in the branch with the unstable focal point) appears in the perturbed CCGLE, too.

We have also studied the changes in the fixed point (η_1, k_1) with the change of the bifurcation parameter γ: (a) below the bifurcation value, i.e., $\gamma = \gamma^* = 0.0635$ $(\gamma^* < \gamma_b)$; (b) at bifurcation point $\gamma = \gamma_b = 0.064\,083\,3$; and, finally, (c) above the bifurcation value of $\gamma = \gamma^{**} = 0.0645$ $(\gamma_b < \gamma^{**})$. In all of the above-mentioned cases, it has been established that the fixed point is a saddle. We have also observed a very good correspondence between the results from the numerical solution of Eq. (1) with different initial conditions and the results from the numerical solution of Eq. (1) near the saddle point.

VI. CONCLUSION

We have found long-living periodic solutions of the complex cubic-quintic Ginzburg-Landau equation (CCQGLE) perturbed with intrapulse Raman scattering. To achieve this we have applied a model system of ordinary differential equations (SODE) for the amplitude and frequency. A set of fixed points of the system has been described. A complete phase portrait as well as phase portraits near the fixed points have been built for a proper choice of parameters. We have applied the bifurcation theory proposed in [46–50] for determining the Lyapunov coefficients (values, quantities) which have the advantage of algebraic purity. We have presented a detailed description of the subcritical Poincaré-Andronov-Hopf bifurcation due to the intrapulse Raman scattering that appears at one of the fixed points. The appearance of an unstable limit cycle in the SODE has been established. To check the validity of the obtained results, we have compared them with the results from the numerical solution of the CCQGLE perturbed with intrapulse Raman scattering with an initial condition given by solitonlike pulses. A good quantitative correspondence has been established between the obtained numerical results for the amplitude and frequency of the soliton pulses and the results for these parameters of the bifurcation theory. We have found that the numerically measured characteristics (amplitude, frequency, width, and position) of the propagating solitonlike pulses periodically change when changing the distance with a period determined by the bifurcation analysis. Based on these results we could expect that a bifurcation analysis of the dynamic model can be used to determine the periodic solutions of the CCGLE perturbed with IRS.

ACKNOWLEDGMENT

The work of I.M.U. and S.G.N. was supported by the Bulgarian National Science Fund through Grant No. KP-06-H72/5.

APPENDIX: FIXED POINTS OF SYSTEM (3)

Let A and B have different signs: $AB < 0 < 1/4$. Then,

First case: $A > 0, B < 0$.

In this case only one of the two roots is positive: $\xi_1 = (-1 + \sqrt{1-4AB})/2A,\ \ \xi_1 > 0,\ \ k_1 = -(c_6/c_5)\xi_1$. For the variable η we get $\eta_1 = \sqrt{\xi_1},\ \ \eta_2 = -\sqrt{\xi_1}$. System (4) has two fixed points: (η_1, k_1) and (η_2, k_1).

Second case: $A < 0, \quad B > 0$.

Here also only one root is positive: $\xi_2 = (-1-\sqrt{1-4AB})/2A,\ \ \xi_2 > 0,\ \ k_1 = -(c_6/c_5)\xi_2$. For the variable η we get $\eta_1 = \sqrt{\xi_2},\ \ \eta_2 = -\sqrt{\xi_2}$. System (4) has two fixed points: (η_1, k_1) and (η_2, k_1).

Let now A and B have equal signs.

Third case: $A < 0,\ \ B < 0,\ \ AB < 1/4$.

In this case two roots are positive: $\xi_1 = (-1 + \sqrt{1-4AB})/2A$ and $\xi_2 = (-1-\sqrt{1-4AB})/2A$, correspondingly $k_1 = -(c_6/c_5)\xi_1$ and $k_2 = -(c_6/c_5)\xi_2$. For the variable η we get $\eta_1 = \sqrt{\xi_1},\ \eta_2 = -\sqrt{\xi_1},\ \eta_3 = \sqrt{\xi_2},\ \eta_4 = -\sqrt{\xi_2}$. Therefore System (4) has four fixed points: (η_1, k_1), (η_2, k_1), (η_3, k_2), and (η_4, k_2).

Fourth case: $A > 0,\ \ B > 0,\ \ AB < 1/4$.

In this case $\xi_{1,2} = (-1 \pm \sqrt{1-4AB})/2A < 0$ and System (4) does not have fixed points.

Fifth case: $A < 0,\ \ B < 0,\ \ AB = 1/4$.

In this case $\xi_1 = -(1/2A) > 0$, $k_1 = -(c_6/c_5)\xi_1$. The variable η takes two values: $\eta_1 = \sqrt{\xi_1},\ \eta_2 = -\sqrt{\xi_1}$. Then System (4) has two fixed points: (η_1, k_1), (η_2, k_1).

Sixth case: $A > 0,\ \ B > 0,\ \ AB = 1/4$.

Here $\xi_1 = -(1/2A) < 0$ and System (4) does not have fixed points.

[1] H. A. Haus, Theory of mode locking with a fast saturable absorber, J. Appl. Phys. **46**, 3049 (1975).

[2] H. A. Haus, J. G. Fujimoto, and E. P. Ippen, Structures for additive pulse mode locking, J. Opt. Soc. Am. B **8**, 2068 (1991).

[3] J. D. Moores, On the Ginzburg-Landau laser mode-locking model with fifth-order saturable absorber term, Opt. Commun. **96**, 65 (1993).

[4] M. Matsumoto, H. Ikeda, T. Uda, and A. Hasegawa, Stable soliton transmission in the system with nonlinear gain, J. Lightwave Technol. **13**, 658 (1995).

[5] G. P. Agrawal, *Applications of Nonlinear Fiber Optics* (Academic Press, New York, 2001).

[6] N. R. Pereira and L. Stenflo, Nonlinear Schrödinger equation including growth and damping, Phys. Fluids **20**, 1733 (1977).

[7] Kh. I. Pushkarov, D. I. Pushkarov, and I. V. Tomov, Self-action of light beams in nonlinear media: Soliton solutions, Opt. Quantum Electron. **11**, 471 (1979).

[8] K. Nozaki and N. Bekki, Exact solutions of the generalized Ginzburg-Landau equation, J. Phys. Soc. Jpn. **53**, 1581 (1984).

[9] N. N. Akhmediev, V. M. Eleonskii, and N. E. Kulagin, Exact first-order solutions of the nonlinear Schrödinger equation,Theor. Math. Phys. **72**, 809 (1987).

[10] P. A. Bélanger, L. Gagnon, and C. Pare, Solitary pulses in an amplified nonlinear dispersive medium, Opt. Lett. **14**, 943 (1989).

[11] B. A. Malomed and A. A. Nepomnyashchy, Kinks and solitons in the generalized Ginzburg-Landau equation, Phys. Rev. A **42**, 6009 (1990).

[12] R. Conte and M. Musette, Exact solutions to the complex Ginzburg-Landau equation of nonlinear optics, Pure Appl. Opt. **4**, 315 (1995).

[13] N. N. Akhmediev, V. V. Afanasjev, and J. M. Soto-Crespo, Singularities and special soliton solutions of the cubic-quintic complex Ginzburg-Landau equation, Phys. Rev. E **53**, 1190 (1996).

[14] V. V. Afanasjev, N. N. Akhmediev, and J. M. Soto-Crespo, Three forms of localized solutions of the quintic complex Ginzburg-Landau equation, Phys. Rev. E **53**, 1931 (1996).

[15] J. M. Soto-Crespo, N. N. Akhmediev, and V. V. Afanasjev, Stability of the pulselike solutions of the quintic complex Ginzburg–Landau equation, J. Opt. Soc. Am. B **13**, 1439 (1996).

[16] N. N. Akhmediev and A. Ankiewicz, *Solitons: Nonlinear Pulses and Beams* (Chapman and Hall, London, 1997).

[17] R. Conte and M. Musette, Solitary waves of nonlinear non-integrable equations, in *Dissipative Solitons*, Lecture Notes in Physics Vol. 661, edited by N. Akhmediev and A. Ankiewicz (Springer, Berlin, 2005), pp. 373–406.

[18] J. M. Soto-Crespo, N. N. Akhmediev, V. V. Afanasjiev, and S. Wabnitz, Pulse solutions of the cubic-quintic complex Ginzburg-Landau equation in the case of normal dispersion, Phys. Rev. E **55**, 4783 (1997).

[19] E. Podivilov and V. L. Kalashnikov, Heavily-chirped solitary pulses in the normal dispersion region: New solutions of the cubic-quintic complex Ginzburg-Landau equation, JETP Lett. **82**, 467 (2005).

[20] W. H. Renninger, A. Chong, and F. W. Wise, Dissipative solitons in normal-dispersion fiber lasers, Phys. Rev. A **77**, 023814 (2008).

[21] A. Hasegawa and Y. Kodama, *Solitons in Optical Communications* (Clarendon, Oxford, 1995).

[22] B. A. Malomed, Evolution of nonsoliton and "quasi-classical" wavetrains in nonlinear Schrodinger equation and Korteweg–de Vries equations with dissipative perturbations, Phys. D (Amsterdam) **29**, 155 (1987).

[23] S. Fauve and O. Thual, Solitary waves generated by subcritical instabilities in dissipative systems, Phys. Rev. Lett **64**, 282 (1990).

[24] Y. Kodama and A. Hasegawa, Generation of asymptotically stable optical solitons and suppression of the Gordon-Haus effect, Opt. Lett. **17**, 31 (1992).

[25] A. I. Maimistov, Evolution of solitary waves which are approximately solitons of a nonlinear Schrödinger equation, Zh. Eksp. Teor. Fiz. **104**, 3620 (1993) [J. Exp. Theor. Phys. **77**, 727 (1993)].

[26] E. N. Tsoy, A. Ankiewicz, and N. N. Akhmediev, Dynamical models for dissipative localized waves of the com-

plex Ginzburg-Landau equation, Phys. Rev. E **73**, 036621 (2006).
[27] A. Ankiewicz, Simplified description of soliton perturbation and interaction using averaged complex potentials, J. Nonlinear Opt. Phys. Mater. **4**, 857 (1995).
[28] W. van Saarloos and P. C. Hohenberg, Pulses and fronts in the complex Ginzburg-Landau equation near a subcritical bifurcation, Phys. Rev. Lett. **64**, 749 (1990).
[29] N. Akhmediev and V. V. Afanasjev, Novel arbitrary-amplitude soliton solutions of the cubic-quintic complex Ginzburg-Landau equation, Phys. Rev. Lett. **75**, 2320 (1995).
[30] J. M. Soto-Crespo, N. N. Akhmediev, and G. Town, Interrelation between various branches of stable solitons in dissipative systems-conjecture for stability criterion, Opt. Commun. **199**, 283 (2001).
[31] R. J. Deisler and H. R. Brand, Periodic, quasiperiodic, and chaotic localized solutions of the quintic complex Ginzburg-Landau equation, Phys. Rev. Lett. **72**, 478 (1994).
[32] J. M. Soto-Crespo, N. Akhmediev, and A. Ankiewicz, Pulsating, creeping, and erupting solitons in dissipative systems, Phys. Rev. Lett. **85**, 2937 (2000).
[33] N. N. Akhmediev, J. M. Soto-Crespo, and G. Town, Pulsating solitons, chaotic solitons, period doubling, and pulse coexistence in mode-locked lasers: Complex Ginzburg–Landau equation approach, Phys. Rev. E **63**, 056602 (2001).
[34] G. P. Agrawal, *Nonlinear Fiber Optics* (Academic Press, New York, 1995).
[35] R. H. Stolen, J. P. Gordon, W. J. Tomlinson, and H. A. Haus, Raman response function of silica fibers, J. Opt. Soc. Am. B **6**, 1159 (1989).
[36] V. V. Afanasyev, V. A. Vysloukh, and V. N. Serkin, Decay and interaction of femtosecond optical solitons induced by the Raman self-scattering effect, Opt. Lett. **15**, 489 (1990).
[37] V. N. Serkin, T. L. Belyaeva, G. H. Corro, and M. Aguero Granados, Stimulated Raman self-scattering of femtosecond pulses. I. Soliton and non-soliton regimes of coherent self-scattering, Quantum Electron. **33**, 325 (2003).
[38] L. Song, L. Li, Z. Li, and G. Zhou, Effect of third-order dispersion on pulsating, erupting and creeping solitons, Opt. Commun. **249**, 301 (2005).
[39] H. Tian, Z. Li, Z. Hu, J. Tian, and G. Zhou, Stable soliton in the fiber-optic system with self-frequency shift, J. Opt. Soc. Am. B **20**, 59 (2003).
[40] S. C. V. Latas and M. F. S. Ferreira, Soliton propagation in the presence of intrapulse Raman scattering and nonlinear gain, Opt. Commun. **251**, 415 (2005).
[41] G. S. Parmar, B. A. Malomed, and S. Jana, Interplay of multiphoton absorption, Raman scattering, and third-order dispersion in soliton fiber lasers, J. Opt. Soc. Am. B **38**, 342 (2021).
[42] S. C. Latas, M. F. S. Ferreira, and M. V. Facao, Impact of higher-order effects on pulsating, erupting and creeping solitons, Appl. Phys. B **104**, 131 (2011).
[43] S. C. Latas and M. F. Ferreira, Emerging fixed-shape solutions from a pulsating chaotic soliton, Opt. Lett. **37**, 3897 (2012).
[44] I. M. Uzunov, Z. D. Georgiev, and T. N. Arabadzhiev, Influence of intrapulse Raman scattering on stationary pulses in the presence of linear and nonlinear gain as well as spectral filtering, Phys. Rev. E **90**, 042906 (2014).
[45] I. M. Uzunov, Z. D. Georgiev, and T. N. Arabadzhiev, Transitions of stationary to pulsating solutions in the complex cubic-quintic Ginzburg-Landau equation under the influence of nonlinear gain and higher-order effects, Phys. Rev. E **97**, 052215 (2018).
[46] A. A. Andronov, E. A. Leontovich, I. I. Gordon, and A. G. Maier, *Theory of Bifurcations of Dynamical Systems on the Plane* (Wiley, New York, 1973).
[47] N. Bautin and E. Leontovich, *Methods and Rules for the Qualitative Study of Dynamical Systems on the Plane* (Nauka, Moscow, 1976).
[48] S. Wiggins, *Introduction to Applied Nonlinear Dynamical Systems*, 2nd ed. (Springer, New York, 2003).
[49] Yu. Kuznetsov, *Elements of Applied Bifurcation Theory*, 2nd ed. (Springer, New York, 1998).
[50] L. Shilnikov, A. Shilnikov, D. Turaev, and L. Chua, *Methods of Qualitative Theory in Nonlinear Dynamics, Part 2* (World Scientific, London, 2001).
[51] M. J. Potasek, G. P. Agrawal, and S. C. Pinault, Analytical and numerical study of pulse broadening in nonlinear dispersive optical fibers, J. Opt. Soc. Am. B **3**, 205 (1986).
[52] I. M. Uzunov and T. N. Arabadzhiev, On the efficiency of different numerical methods for the calculation of intrapulse Raman scattering of optical solitons, Opt. Quantum Electron. **51**, 283 (2019).
[53] M. Erkinalo, G. Genty, B. Wetzel, and J. M. Dudley, Limitations of the linear Raman gain approximation in modeling broadband nonlinear propagation in optical fibers, Opt. Express **18**, 25449 (2010).
[54] V. L. Kalashnikov and A. Apolonski, Chirped-pulse oscillators: A unified standpoint, Phys. Rev. A **79**, 043829 (2009).
[55] A. Komarov, H. Leblond, and F. Sanchez, Quintic complex Ginzburg-Landau model for ring fiber lasers, Phys. Rev. E **72**, 025604(R) (2005).
[56] V. E. Zakharov and A. B. Shabat, Exact theory of two-dimensional self-focusing and one-dimensional self-modulation of waves in nonlinear media, Zh. Eksp. Teor. Fiz. **61**, 118 (1971) [Sov. Phys. JETP **34**, 62 (1972)].
[57] Wolfram *Mathematica 8*, Wolfram Research, Inc. (2010).
[58] L. Shilnikov, Theory of bifurcation of dynamical systems and dangerous boundaries, Dokl. Akad. Nauk SSSR **224**, 1046 (1975) [Math. Phys. **20**, 674 (1975)].
[59] J. M. T. Thompson, H. B. Stewart, and Y. Ueda, Safe, explosive, and dangerous bifurcations in dissipative dynamical systems, Phys. Rev. E **49**, 1019 (1994).
[60] T. Kapitula and B. Sandstede, Instability mechanism for bright solitary-wave solution to the cubic-quintic Ginzburg-Landau equation, J. Opt. Soc. Am. B **15**, 2757 (1998).
[61] D. Arrowsmith and C. Place, *Dynamical Systems. Differential Equations, Maps and Chaotic Behavior* (Chapman & Hall, London, 1992).